# Wiley Analytical Science

The Current State of Reconstruction Technologies for 3D X-ray Microscopy including Algorithmic Innovation for AI-based Recovery

April 26, 10:00am - 11:00am EDT

Many properties can only be fully understood in 3D, such as porosity and tortuosity in porous materials, network connection maps in neuroscience, or mechanical properties in 3D additively manufactured structures. X-ray microscopy provides a unique method to image samples non-destructively in 3D across a wide range of materials and life sciences.

Watch this session during the WAS Virtual Conference:
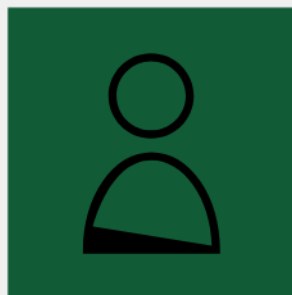
Nicolas Guenichault, Ph.D.   **Dr. Stephen T. Kelly, Ph.D.**

Register Now

This talk is sponsored by **ZEISS**

Pro-Peptide-Reinforced, Mucus-Penetrating Pulmonary siRNA Delivery Mitigates Cytokine Storm in Pneumonia

Jiandong Yang, Shanzhou Duan, Huan Ye, Chenglong Ge, Chunxian Piao, Yongbing Chen, Minhyung Lee, and Lichen Yin*

Pulmonary delivery of anti-inflammatory siRNA holds great potential in mitigating the cytokine storm during severe pneumonia. However, commonly utilized polycationic siRNA delivery vehicles can hardly penetrate the mucus barrier, thus greatly hurdling their therapeutic efficacy. Herein, TNF-α siRNA (siTNF-α) delivery nanocomplexes (NCs) are engineered with mucus/cytomembrane dual-penetration capabilities, realized via surface-coating of NCs with RC, an inflammation-sheddable, charge-reversal pro-peptide of RAGE-binding peptide (RBP). RC-coated dendritic poly-L-lysine/siTNF-α (DsT) NCs possess negative surface charges, and can thus efficiently penetrate the mucus layer after intratracheal administration. In the inflamed alveolar space with mild acidity, RC recovers to the cationic RBP and shed off, re-exposing the DsT NCs that efficiently transfect the alveolar macrophages and provokes TNF-α silencing. Thus, siTNF-α and RBP cooperatively alleviate the uncontrolled inflammation during acute lung injury. This study renders a unique approach for mediating trans-mucus nucleic acid delivery, and will find promising utilities for the treatment of severe pneumonia.

1. Introduction

Pneumonia is one of the most common infectious diseases. It can be caused by various direct or indirect factors, such as the corona virus 2019 (COVID-19) that has infected over 38 million people and killed more than 1 million so far.

J. Yang, H. Ye, C. Ge, Prof. L. Yin
Institute of Functional Nano & Soft Materials (FUNSOM)
Jiangsu Key Laboratory for Carbon-Based Functional Materials & Devices
Collaborative Innovation Center of Suzhou Nano Science & Technology
Soochow University
Suzhou 215123, China
E-mail: lcyin@suda.edu.cn
Dr. S. Duan, Prof. Y. Chen
Department of Thoracic Surgery
The Second Affiliated Hospital of Soochow University
Suzhou 215002, China
Dr. C. Piao, Prof. M. Lee
Department of Bioengineering
College of Engineering
Hanyang University
Seoul 04763, Korea

The ORCID identification number(s) for the author(s) of this article can be found under https://doi.org/10.1002/adfm.202008960.

Severe pneumonia can cause acute lung injury (ALI)/acute respiratory distress syndrome (ARDS), which is associated with high morbidity and mortality.[1] ALI/ARDS stems from an aggressive pro-inflammatory response and insufficient anti-inflammatory response, thus leading to the uncontrolled inflammatory process, known as the fulminant cytokine storm.[2] The severe inflammation leads to serious pathological complications, such as diffuse alveolar damage, progressive collagen deposition, fibrin exudates, fibrotic healing, etc.[3] Moreover, the pulmonary cytokine storm will spill over into the circulation, inducing systemic cytokine storm and ultimately leading to multi-organ dysfunction. During the initiation and cascade of cytokine storm, a spectrum of pro-inflammatory cytokines is over-produced, among which tumor necrosis factor-α (TNF-α) plays a prominent role in the cytokine storm and is closely related to the escalation of inflammatory severity.[2,3] As such, down-regulation of pro-inflammatory cytokines, especially TNF-α, holds huge potentials for the anti-inflammation therapy against ALI/ARDS via inhibition of the cytokine storm.

Small interfering RNA (siRNA)-mediated gene silencing against pro-inflammatory cytokines provides a promising modality for anti-inflammatory treatment, benefiting from the sequence-specific mRNA degradation at high efficiency and specificity.[4–7] To realize the therapeutic performance of siRNA in vivo, a potent carrier administered via an appropriate route is highly demanded.[8–19] Polycations are an important category of siRNA delivery materials which can condense siRNA into positively charged nanocomplexes (NCs) to facilitate cellular internalization and transfection.[20–24] Local intratracheal delivery to the lung features distinct advantages for the treatment of pulmonary diseases, such as immediate availability and minimal systemic side effect.[25–28] However, the performance of intratracheally administered NCs is often greatly hurdled by the viscous mucus layer covering the airway.[29,30] Mucus is secreted by goblet epithelial cells and is composed of negatively charged mucin monomers that crosslink to form the mesh-like architecture through disulfide bonds.[31] The mucin glycoprotein imparts strong electrostatic interactions with the positively charged NCs, which thus traps the NCs in the mucus matrix followed by fast muco-ciliary clearance,

ultimately preventing the NCs from reaching the underlying alveolar spaces.[32,33] The mucus secretion becomes even pronounced in patients suffering from severe pulmonary inflammation (such as critical patients of COVID-19), which dramatically compromises the therapeutic efficacy in the way of intratracheal administration and inhalation.[34] As such, siRNA delivery systems with potent mucus-penetrating capabilities are highly imperative toward the success of pulmonary gene silencing.

High-density PEGylation of polycations serves to efficiently promote the mucus permeation, a pioneering strategy reported by Hanes and co-workers.[35,36] Commercialized polycations (PEI and dendrimer) modified with a high-density PEG layer displayed enhanced mucus permeation capabilities, mainly due to the diminished electrostatic adhesive interaction with the mucus.[37] Nevertheless, the dense PEG layer may in the meantime compromise the cellular uptake and gene transfection efficiencies.[38] Surface-decoration of the NCs with negatively charged shell can also facilitate the diffusion across the mucus layer because the modified NCs enabled electrostatic repulsion toward the mucin glycoproteins. However, the efficiencies of internalization, as well as endolysosomal escape in target cells, still remain doubtful, unless an efficient shell-shedding mechanism is adopted.[39–42] To the best of our knowledge, siRNA delivery systems that can harmonize the processes of mucus transport and cellular/endolysosomal membrane penetration are still highly lacking.

To address the dearth of techniques for pulmonary siRNA delivery, we herein report the design of mucus and cell membrane dual-penetrating NCs that are capable of inflammation-instructed charge reversal from negative to positive as assisted by an acid-sheddable pro-peptide. Dendritic poly-L-lysine (DPLL) was first developed to condense TNF-α siRNA (siTNF-α) and form the positively charged DPLL/siTNF-α (DsT) NCs. RAGE-binding peptide (RBP), a cationic antagonist to the receptor for advanced glycation end products (RAGE) that can block the interaction between RAGE and its ligands and down-regulate pro-inflammatory factors,[43–45] was reversibly modified with cis-aconitic anhydride (CA) to afford the negatively charged pro-peptide, RBP-cis-aconitic amide (RC), which was utilized to coat the DsT NCs. The obtained RC/DPLL/siTNF-α (RCDsT) NCs possessed negative surface charges, thereby allowing efficient mucus penetration upon intratracheal administration. Upon reaching the inflamed alveolar spaces with mildly acidic environment (pH $\approx$6.8), RC transformed back to the positively charged RBP, which shed off as a result of electrostatic repulsion.[39,46] The exposed DsT NCs with positive surface charges could then efficiently transfect the alveolar macrophages to mediate TNF-α silencing.[47,48] In the meantime, the reactivated RBP bound to RAGE on inflamed macrophage membranes and thereafter down-regulated the various pro-inflammatory cytokines such as TNF-α, interleukin-1β (IL-1β), interleukin-6 (IL-6), etc.[43–45] Such an inflammation-sheddable pro-peptide not only provides an effective approach to solve the dilemma between mucus penetration and cellular uptake but also cooperates with siTNF-α to alleviate the cytokine storm toward ALI treatment (**Figure 1**).

2. Results and Discussion

2.1. Preparation, Characterization, and Acid-responsiveness of RCDsT NCs

Firstly, DPLL was synthesized via ring-opening polymerization (ROP) of $N(\varepsilon)$-benzyloxycarbonyl-L-lysine-N-carboxyanhydride (zLL-NCA) as initiated by third-generation PAMAM (G3-PAMAM) followed by removal of the Boc protection groups (Figure S1A, Supporting Information). The chemical structures of the zLL-NCA monomer, dendritic poly-zLL (DPzLL), and DPLL were characterized by ^{1}H NMR (Figure S1B–D, Supporting Information). Gel permeation chromatography analysis revealed that the number-average molecular weight (M_n) of DPzLL was 480.0 kDa, with the polydispersity index of 1.07. The pH-sensitive RC was synthesized via ring-opening reaction of CA with RBP at pH 8.5. The non-responsive RBP-glutaric amide (RG) was similarly synthesized from RBP and glutaric anhydride (GA, Figure S2, Supporting Information). MALDI-TOF analysis revealed that the grafting ratio of CA in RC was ≈60%, while that of GA in RG was around ≈80%. The pH-responsive RC but not the non-responsive RG could recover to the original relative molecular mass (M_r) after incubation at pH 6.8 for 30 min (**Figure 2**A and Figure S3, Supporting Information). In consistence, the zeta potential of RC but not RG recovered from negative to positive after incubation at pH 6.8 for 30 min (Figure 2A), and RC but not RG revealed similar anti-inflammatory effect to the native RBP in inhibiting lipopolysaccharide (LPS)-induced TNF-α secretion in RAW 264.7 cells at pH 6.8 (Figure S4, Supporting Information). It thus demonstrated the charge reversal and re-activation of RC in response to mild acidity.

Then, DPLL was allowed to form the binary DsT NCs with siTNF-α, followed by surface coating with RC via electrostatic interaction to obtain the ternary RCDsT NCs. The siTNF-α condensation ability of DPLL was assessed by the gel retardation assay. DPLL was able to condense siTNF-α at the DPLL/siTNF-α weight ratio ≥2, as indicated by the retardation of siTNF-α in the loading well (Figure S5A, Supporting Information). Particle size of the binary DsT NCs gradually decreased while zeta potential gradually increased when the DPLL/siTNF-α weight ratio increased. At the weight ratio of 5, binary NCs with diameter of ≈150 nm and positive zeta potential of ≈7 mV were obtained (Figure 2C,D, and Figure S6A, Supporting Information). When the DsT NCs (DPLL/siTNF-α = 5, w/w) were coated with RC at incremental RC/siTNF-α weight ratios from 1 to 40, particle size of the RCDsT ternary NCs maintained smaller than 200 nm while the zeta potential continuously decreased to −12 mV at the RC/siTNF-α weight ratio of 40 (Figure 2E,F, and Figure S6B, Supporting Information). Gel retardation assay revealed lack of siTNF-α migration after agarose gel electrophoresis at all tested RC/siTNF-α weight ratios (Figure S5B, Supporting Information), indicating that siTNF-α was not repelled out of the NCs after surface coating with RC. Also, after the RCDsT NCs (w/w/w = 40/5/1) were incubated with purulent sputum obtained from cystic fibrosis (CF) patients for up to 4 h, no siRNA migration was observed after agarose gel electrophoresis (Figure S7, Supporting Information),
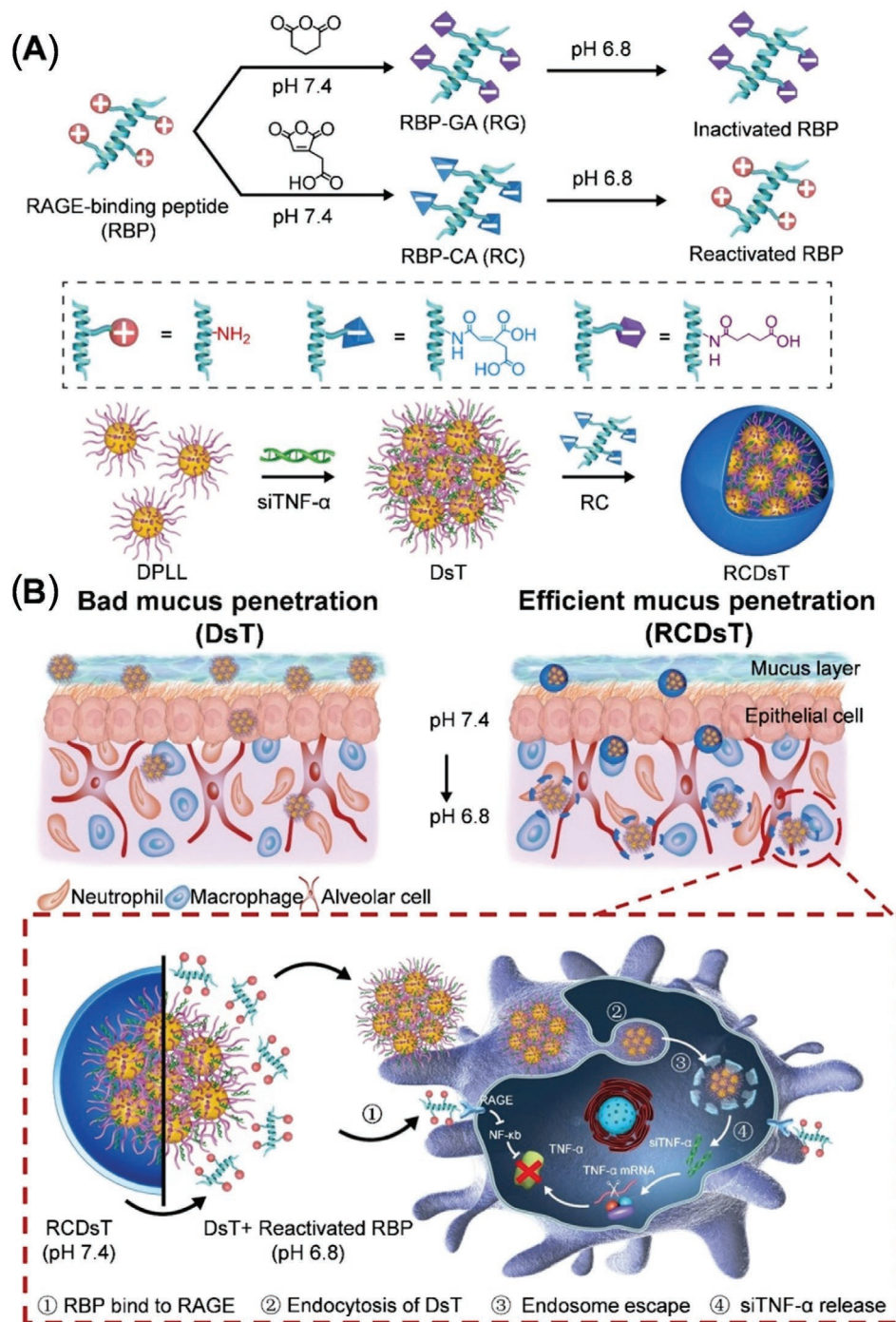
Figure 1. Schematic illustration of the acid-sensitive, charge-reversible RCDsT NCs capable of potent mucus and macrophage membrane penetration. siTNF-α is condensed by DPLL to form the binary DsT NCs which are further coated with RC, the acid-responsive pro-peptide of RBP, to form the ternary RCDsT NCs. After intratracheal administration, RCDsT NCs with negative surface charges efficiently penetrated the mucus layer due to their electrostatic repulsion with mucin glycoproteins. When they reached the inflamed alveolar spaces with mild acidity, RC transformed back to the positively charged RBP, which detached from the NCs and re-exposed the positively charged DsT NCs. The reactivated RBP bound to RAGE on inflamed macrophage membrane to inhibit pro-inflammatory factors while the DsT NCs mediated effective TNF-α silencing, thus contributing to the cooperative anti-inflammatory effect against the cytokine storm during LPS-challenged ALI.

indicating encapsulation of the siRNA inside the NCs. Such property would allow the NCs to maintain integrity after crossing the mucus barrier. NCs comprised of the negative control siRNA (siNC) or the non-responsive RG were similarly prepared, and the abbreviations for all tested NCs were listed in Table S1, Supporting Information.
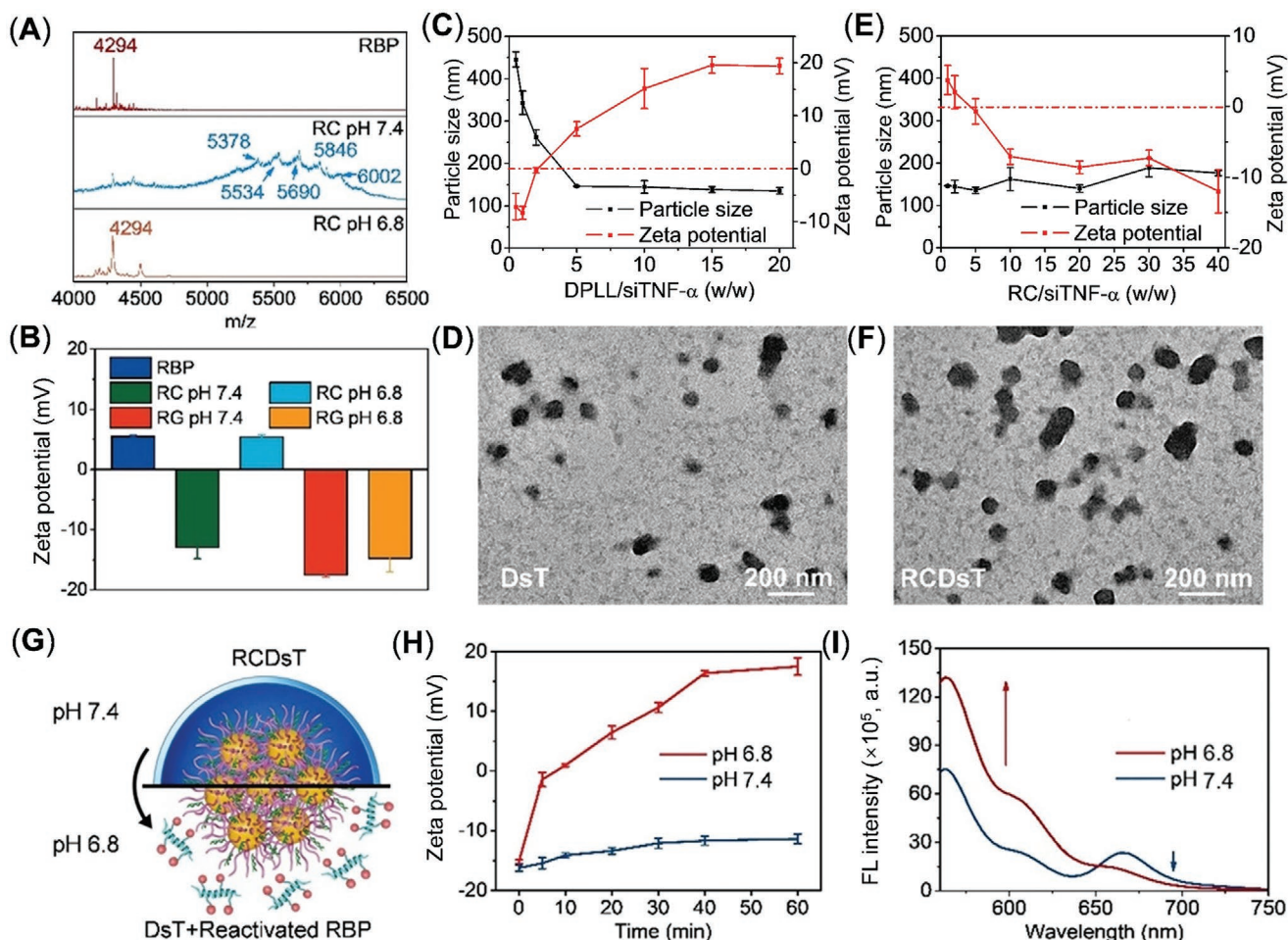
Figure 2. pH-responsive transformation of RC and RCDsT NCs. A) MALDI-TOF analysis of RBP, RC at pH 7.4, and RC at pH 6.8. B) Zeta potential of RBP, pH-responsive RC, and non-responsive RG at pH 7.4 and 6.8. C) Size and zeta potential of the DsT NCs at different DPLL/siTNF-α weight ratios ($n = 3$). D) TEM image of DsT NCs (DPLL/siTNF-α = 5/1, w/w). E) Size and zeta potential of the RCDsT NCs at different RC/siTNF-α weight ratios (DPLL/siTNF-α = 5/1, w/w, $n = 3$). F) TEM image of RCDsT NCs (RC/DPLL/siTNF-α = 40/5/1, w/w/w). G) Mechanistic illustration showing the detachment of RC from the RCDsT NCs surface and re-exposure of the positively charged DsT NCs as a consequence of acid-induced transformation of the negatively charged RC back to the positively charged RBP. H) Zeta potential of the RCDsT NCs after incubation at pH 7.4 or 6.8 for different time ($n = 3$). I) FRET analysis of the RCDsT NCs at pH 7.4 or 6.8. RC is doped with Cy5 and siRNA is labeled with Cy3. The fluorescence recovery of the donor (Cy3, $\lambda_{ex} = 550$ nm) is used to monitor the detachment of RC from the RCDsT NCs.

The charge reversal ability of RCDsT NCs under the mildly acidic condition of the inflammatory site was then explored. The negative zeta potentials of RCDsT NCs maintained almost constant within 1 h at pH 7.4, while it obviously increased and reversed to positive within 20 min at pH 6.8, demonstrating the charge reversal of the RC outer layer and exposure of the positively charged, inner DsT NCs (Figure 2G,H). As a non-responsive control, RGDsT NCs maintained similar and negative zeta potentials at both pH 7.4 and 6.8 (Figure S8, Supporting Information). The fluorescence resonance energy transfer (FRET) assay was further adopted to detect the acid-triggered dissociation of RCDsT NCs comprised of Cy3-siRNA and Cy5-labeled RC. The fluorescence intensity of Cy5 at pH 7.4 was notably higher than that at pH 6.8, and there was an obvious Cy3 fluorescence recovery at pH 6.8 (Figure 2I). This phenomenon revealed that these two dyes in RCDsT NCs, Cy3, and Cy5, were in sufficient proximity to induce FRET at pH 7.4, while they were

separated over distance at pH 6.8 such that the FRET effect was alleviated. In comparison, the fluorescence spectrum of RGDsT NCs comprised of Cy3-siRNA and Cy5-labeled RG maintained similar at both pH 7.4 and 6.8 (Figure S9, Supporting Information). Such discrepancy further substantiated the removal of the RC outer layer from RCDsT NCs at pH 6.8, as a consequence of the mild acidity-triggered charge reversal of RC.

2.2. Cellular Uptake and Intracellular Kinetics of NCs in Macrophages In Vitro

The gene silencing efficiency of siRNA was closely associated with the cellular internalization level and intracellular kinetics of the NCs. Thus, the uptake level of the pH-responsive RCDsT NCs and the non-responsive RGDsT NCs containing FAM-siRNA were first evaluated in RAW 264.7 cells at pH 6.8 or 7.4 by
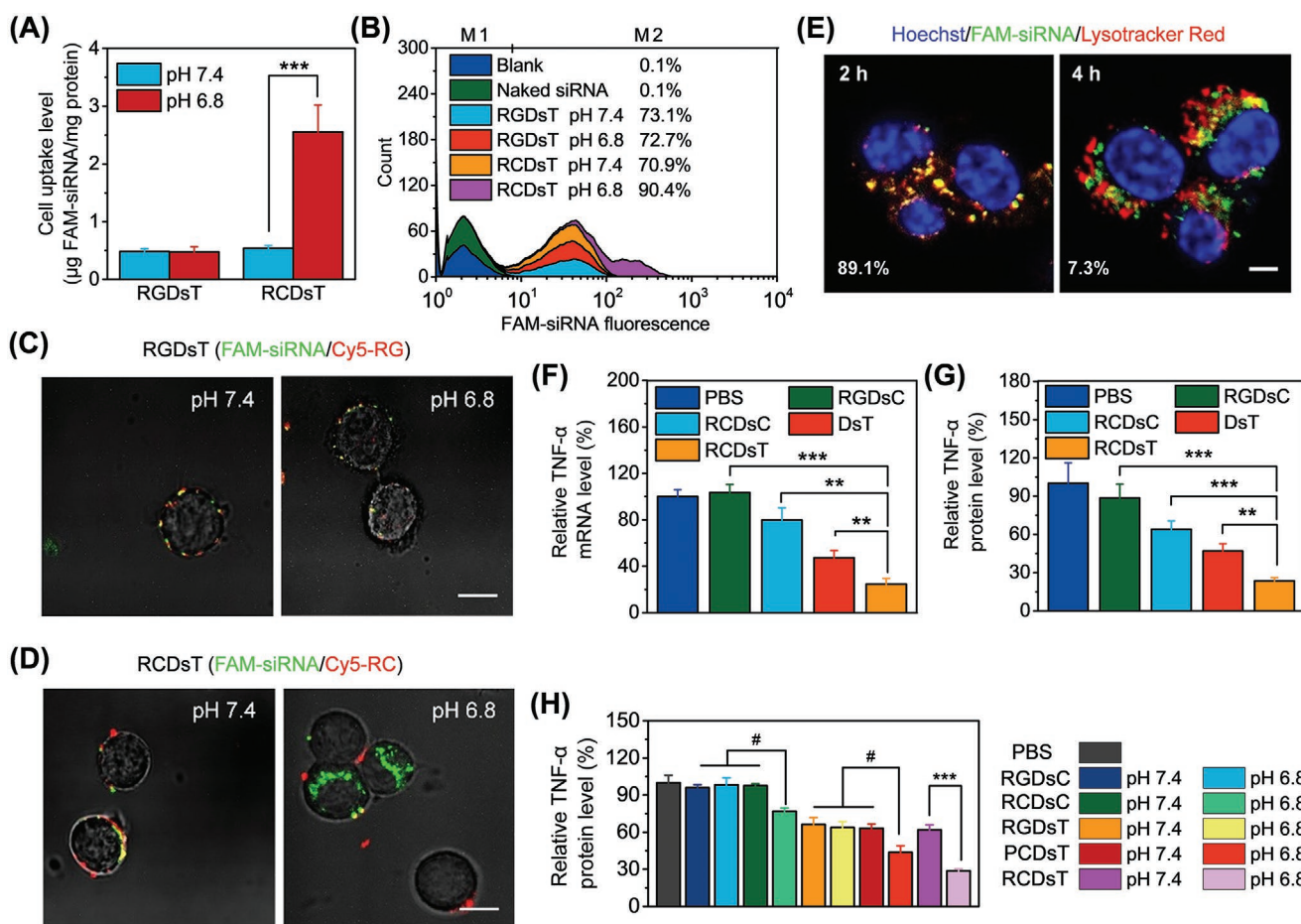
Figure 3. Intracellular kinetics and anti-inflammatory efficacy mediated by various NCs in RAW 264.7 cells in vitro. A) Uptake levels of RGDsT NCs or RCDsT NCs in RAW 264.7 cells at 2 μg FAM-siRNA/mL at pH 7.4 and 6.8 ($n = 3$). B) Flow cytometric analysis of RAW 264.7 cells after 4-h incubation with RGDsT NCs or RCDsT NCs at 2 μg FAM-siRNA/mL at pH 7.4 and 6.8 ($n = 3$). CLSM images of RAW 264.7 cells treated with RGDsT NCs (C) or RCDsT NCs (D) at pH 7.4 and 6.8 (bright field). FAM-siRNA and Cy5-RC (or Cy5-RG) are used to construct the NCs (scale bar = 5 μm). E) CLSM images of RAW 264.7 cells treated with RCDsT NCs containing FAM-siRNA at pH 6.8 for 2 and 4 h. Cell nuclei are stained with Hoechst 33 258, and endolysosomes are stained with Lysotracker Red (scale bar = 5 μm). Relative TNF-α mRNA levels (F) and TNF-α protein levels (G) in RAW 264.7 cells after incubation with different NCs (RGDsC, RCDsC, DsT, and RCDsT) at pH 6.8 as determined by real-time PCR and ELISA, respectively ($n = 3$). H) TNF-α protein levels in RAW 264.7 cells after treatment with different NCs (RGDsC, RCDsC, PCDsT, RGDsT, and RCDsT) at pH 7.4 and 6.8 as determined by ELISA ($n = 3$). Cells are incubated with NCs at 1 μg siRNA/mL for 4 h, further cultured in fresh medium for 20 h, challenged with LPS (7.5 ng mL^{-1}) for 5 h, and then subjected to real-time PCR or ELISA measurements in (F–H).

spectrofluorimetry. The uptake level of RCDsT NCs at pH 6.8 was 5-fold higher than that at pH 7.4, while RGDsT NCs showed similar uptake levels at pH 7.4 and 6.8 (**Figure 3**A). Such a pH-dependent internalization performance of RCDsT NCs could be attributed to the acid-triggered charge reversal and shedding of the RC outer layer, which exposed the positively charged binary DsT NCs to facilitate trans-membrane delivery. Consistent results were obtained from flow cytometric analysis (Figure 3B and Figure S10, Supporting Information). MH-S, a mouse alveolar macrophage cell line, was further used to evaluate the pH-dependent uptake level of NCs, and similar results were noted to those for RAW 264.7 cells (Figure S11, Supporting Information).

Then, the de-shielding of the RC outer layer in the extracellular compartment and the intracellular delivery of the binary DsT NCs were further confirmed by confocal laser scanning microscopy (CLSM) observation. When RAW 264.7 cells were

incubated with RCDsT NCs comprised of FAM-siRNA and Cy5-RC at pH 6.8, only the green fluorescence of FAM-siRNA was spread into the cytoplasm while the red fluorescence of Cy5-RC was still situated on the cell membrane. For the non-responsive RGDsT NCs, the green fluorescence of FAM-siRNA and red fluorescence of Cy5-RG overlapped and was localized on cell membranes (Figure 3C,D). Such disparity thus demonstrated removal of the RC outer layer from RCDsT NCs under mildly acidic condition in the extracellular compartment, which subsequently allowed effective internalization of the DsT NCs. It was further noted that the internalized siRNA cargo was also able to escape from endolysosomal entrapment, as evidenced by the obvious separation of green fluorescence (FAM-siRNA) from red fluorescence (Lysotracker Red-stained endolysosomes) after 4-h incubation (Figure 3E). Such endolysosomal escape potency would potentially benefit efficient gene transfection.

**ADVANCED
SCIENCE NEWS**
www.advancedsciencenews.com

**ADVANCED
FUNCTIONAL
MATERIALS**
www.afm-journal.de

2.3. Gene Silencing Efficiency of NCs in Macrophages In Vitro

In order to demonstrate the siTNF-α-mediated gene silencing efficiency and its combinational anti-inflammatory effect with RBP, the TNF-α mRNA and protein levels in LPS-challenged RAW 264.7 cells were first evaluated by real-time PCR and ELISA, respectively. The TNF-α mRNA level was inhibited by ≈20% or ≈50% after treatment with RCDsC NCs (RBP effect only) or DsT NCs (siTNF-α effect only), respectively, at pH 6.8. Comparatively, RCDsT NCs provoked significantly higher TNF-α mRNA silencing level by ≈75%, which indicated that RBP and siTNF-α had a cooperative anti-inflammatory effect (Figure 3F). In consistence, RCDsT NCs efficiently suppressed the TNF-α secretion level by ≈80%, outperforming RCDsC NCs (≈30%) and DsT NCs (≈50%) (Figure 3G). Similar results were observed in MH-S cells in terms of the TNF-α mRNA down-regulation efficiencies (Figure S12, Supporting Information). The pH-dependent anti-inflammatory efficiencies of NCs were further probed at pH 6.8 and 7.4. In order to elucidate the contribution of charge reversal in potentiating RNAi, poly-L-lysine conjugated with CA (PLL-CA, PC) was synthesized as an analog of RC yet deprived of the pharmacological activity of the peptide (Figure S13, Supporting Information). Similar to RCDsT NCs, the obtained PCDsT NCs also possessed negative surface charges and allowed acid (pH 6.8)-triggered charge reversal. The TNF-α level was inhibited by ≈20% after treatment with RCDsC NCs at pH 6.8, while the RCDsC NCs at pH 7.4 showed negligible TNF-α knockdown efficiency, indicating the acid-induced re-activation of RBP. In support of such observation, RGDsC NCs that were non-responsive to acid failed to down-regulate TNF-α at either pH 7.4 or 6.8. PCDsT NCs exhibited significantly higher TNF-α silencing level at pH 6.8 (≈55%) than at pH 7.4 (≈35%), which demonstrated the contribution of acid-induced charge reversal in potentiating the intracellular siTNF-α delivery efficiency and TNF-α silencing efficiency. Moreover, RCDsT NCs showed comparable TNF-α down-regulation level to PCDsT NCs at pH 7.4 while significantly higher TNF-α down-regulation level than PCDsT NCs at pH 6.8 (Figure 3H). Such discrepancy further demonstrated the mild acidity-promoted gene silencing and re-activation of RBP, which cooperated to enable TNF-α down-regulation in LPS-challenged macrophages. Furthermore, DsT NCs and RCDsT NCs showed negligible cytotoxicity at increased DPLL concentrations up to 40 μg mL^{-1}, indicating their desired cytocompatibility in both RAW 264.7 and MH-S cells (Figures S14 and S15, Supporting Information).
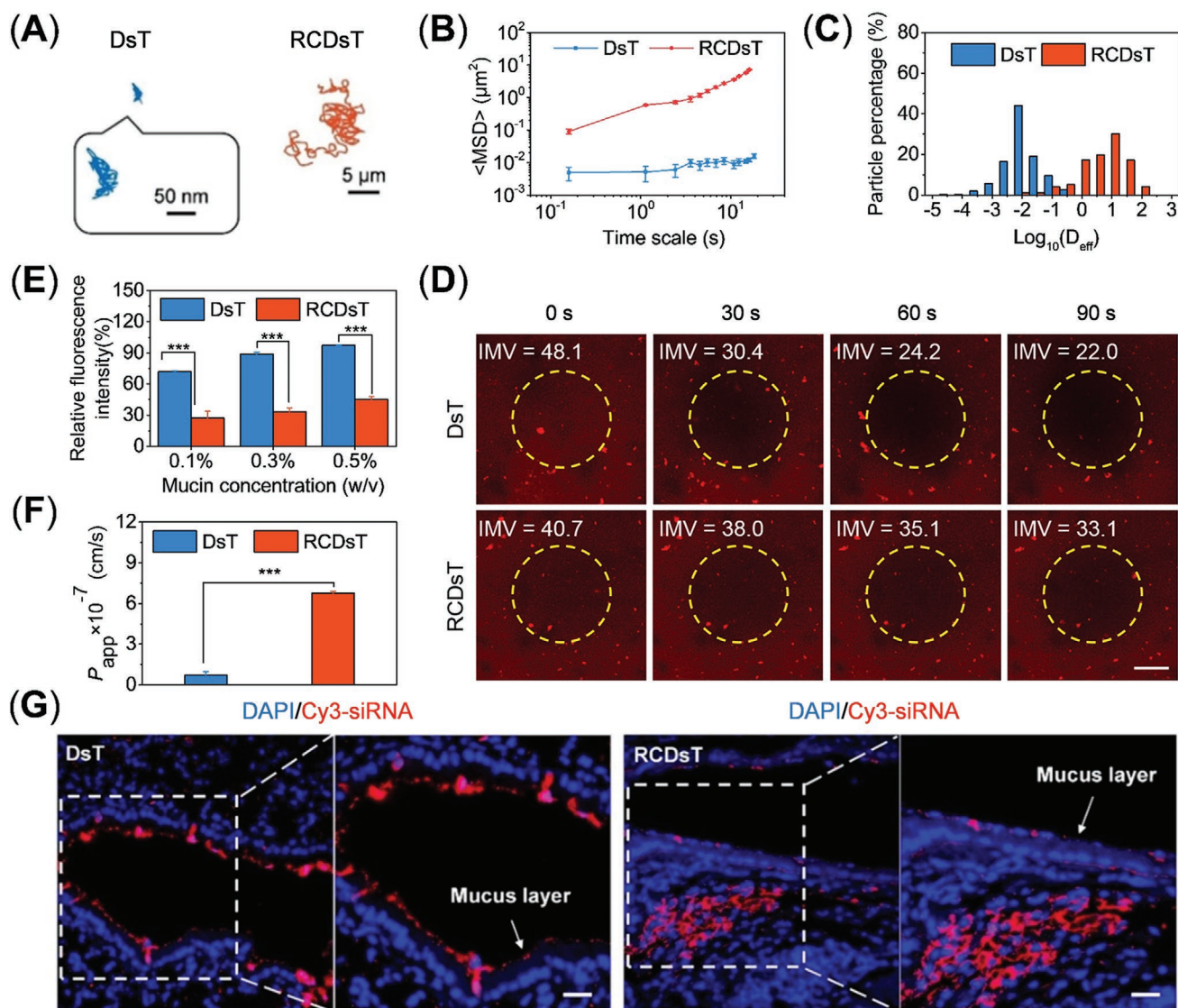
2.4. Mucus Penetration of NCs In Vitro and In Vivo

To enable anti-inflammation performance in lung tissues upon intratracheal administration, NCs should be able to penetrate the mucus layer with high efficiency to reach the underlying epithelia and macrophages. Herein, multiple particle tracking (MPT) assay was first adopted to determine the translational motion of DsT NCs or RCDsT NCs containing Cy3-siRNA in purulent sputum obtained from CF patients.[29,35] The Brownian movement of the positively charged DsT NCs was greatly hindered in CF sputum while that of the negatively charged RCDsT NCs was more drastic (**Figure** 4A). Consistently, the mean square displacement (⟨MSD⟩) value of RCDsT NCs was about 1000-fold higher than that of DsT NCs at 10 s (Figure 4B), and majority of RCDsT NCs possessed uniformly higher effective diffusivities (D_{eff}) than DsT NCs (Figure 4C).

The translational motion of NCs in purulent sputum was further evaluated using the photobleaching assay.[49] The extent of the fluorescence intensity decreased in the yellow circle during photobleaching negatively correlates to the efficiency of the diffusive spreading of the Cy3-siRNA-containing NCs. The fluorescence decrease percentage of DsT NCs (≈54%) was about 3-fold higher than that of RCDsT NCs (≈19%) at 90 s, indicating the remarkably stronger diffusive capability of RCDsT NCs, which could be ascribed to their negatively charged surfaces that prevented adsorption of negatively charged mucin glycoproteins (Figure 4D). In support of such hypothesis, the interactions between NCs and mucin glycoproteins were explored using the mucin aggregation assay.[29] About 70–95% of mucin glycoproteins aggregated with DsT NCs at all tested mucin concentrations, while in comparison, a dramatically lower amount of mucin glycoproteins (30–45%) aggregated with RCDsT NCs (Figure 4E). These results thus collectively substantiated that the RC coating on the binary DsT NCs reduced the adsorption of mucin glycoproteins by transforming the surface charge of NCs from positive to negative, which thus facilitated the diffusion of RCDsT NCs in the mucus layer.

The trans-mucus delivery efficiency of NCs was then evaluated in vitro in the air-interfaced culture (AIC) of Calu-3 cells, a well-established model of bronchial epithelia that forms dense cell monolayer framework with sufficient secreted mucus.[50] Cy3-siRNA was used to form DsT NCs and RCDsT NCs, and their transport levels across cell monolayers were represented by the apparent permeability coefficient (P_{app}) of Cy3-siRNA. The P_{app} of Cy3-siRNA in RCDsT NCs was almost seven-fold higher than that of Cy3-siRNA in DsT NCs, indicating stronger trans-mucus and trans-epithelial delivery efficiency of the RCDsT NCs (Figure 4F). The TEER values of Calu-3 cell monolayers before addition of DsT NCs and RCDsT NCs were 738.0 ± 25.9 and 780.3 ± 24.7 Ω·cm^2 (n = 3), respectively, and they showed no significant change after the 4-h transport study (750 ± 17.8 and 784.2 ± 35.0 Ω·cm^2, n =3). Such a result indicated that the monolayers remained intact after exposure to NCs. Moreover, RCDsT NCs that had been transported across the Calu-3 cell monolayers were collected and used to transfect MH-S cells. As shown in Figure S16, Supporting Information, there was no significant difference between freshly prepared NCs and the transported NCs, indicating that the transported NCs could still maintain their transfection capability. Furthermore, CLSM was utilized to observe the mucus penetration behavior of NCs in vivo after intratracheal administration. The red fluorescence of Cy3-siRNA in DsT NCs was mainly distributed over the side of goblet cells, indicating entrapment of the positively charged DsT NCs in the mucus layer lining above the epithelia. In obvious contrast, majority of the RCDsT NCs were distributed into deeper regions of lung tissues (Figure 4G). It thus demonstrated that the RCDsT NCs afforded potent trans-mucus delivery properties, mainly benefiting from their negatively charged surfaces. In consistence with such finding, ex vivo imaging of major organs further revealed that the

Figure 4. RCDsT NCs mediate potent mucus penetration in vitro and in vivo. A) Representative trajectories of Cy3-siRNA-containing DsT NCs and RCDsT NCs in the CF mucus during the 20-s movies. B) The mean square displacements (<MSD>) of individual NCs as a function of the time scale. C) Distribution of the logarithmic effective diffusivities (Log$_{10}$ (D_{eff})) of individual NCs (n > 100 NCs per experiment). D) Representative images of Cy3-siRNA-containing DsT NCs and RCDsT NCs in mucin solution (0.3%, w/v) upon photobleaching for different time (scale bar = 40 μm). The intensity mean values represent the fluorescence intensity in the irradiated region (within yellow circle). E) The percentage of Cy3-siRNA-containing DsT NCs or RCDsT NCs that formed aggregates with mucin glycoproteins at different mucin concentrations (n = 3). The total amount of Cy3-siRNA served as 100%. F) P_{app} of Cy3-siRNA across the AIC model after incubation with Cy3-siRNA-containing DsT NCs or RCDsT NCs for 6 h (n = 3). G) Distribution of Cy3-siRNA-containing DsT NCs and RCDsT NCs in lung epithelial tissues following intratracheal administration. Cell nuclei are stained with DAPI (scale bar = 25 μm).

biodistribution levels of Cy5-siRNA-containing RCDsT NCs in lung tissues were notably higher than those of Cy5-siRNA-containing DsT NCs at 4 h post intratracheal administration (Figure S17, Supporting Information). It again indicated that the negatively charged RCDsT NCs could effectively penetrate the mucus layer and distribute into lung tissues, while the positively charged DsT NCs could be trapped by the mucus layer and get eliminated along with the fast mucus turn-over. At 24 h post-administration, distribution of NCs in the liver and kidney was noted, which may be related to their elimination from the body via biliary and/or urinary excretion.

2.5. Gene Silencing Efficiency and Anti-inflammatory Efficacy of NCs Against Cytokine Storm In Vivo
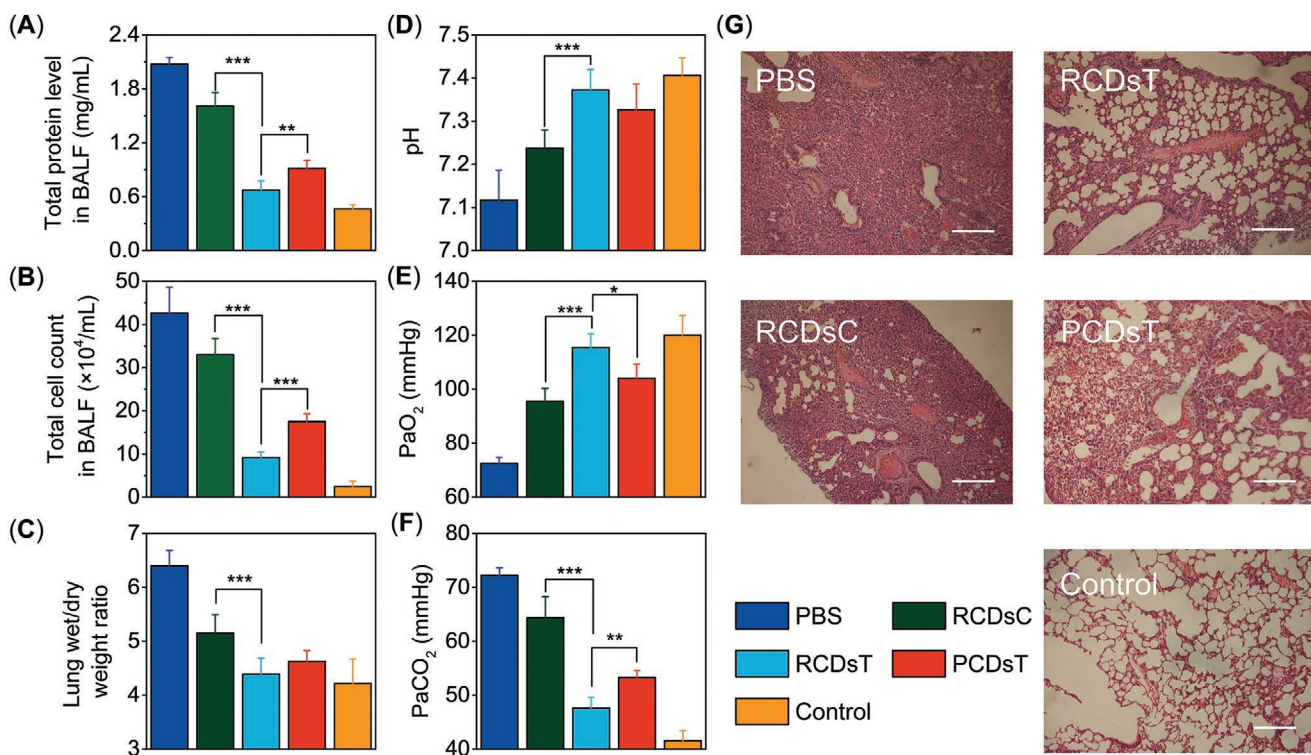
The gene knockdown efficiency and anti-inflammatory efficacy of intratracheally administered NCs were evaluated in LPS-induced ALI mice. The TNF-α mRNA levels in lung tissues were first monitored (**Figure 5**A). PCDsT NCs significantly outperformed DsT NCs in terms of the TNF-α silencing efficiency, demonstrating that the negatively charged NCs facilitated the mucus permeation to consequently potentiate the in vivo gene silencing in inflamed lung tissues. PCDsT NCs with the charge
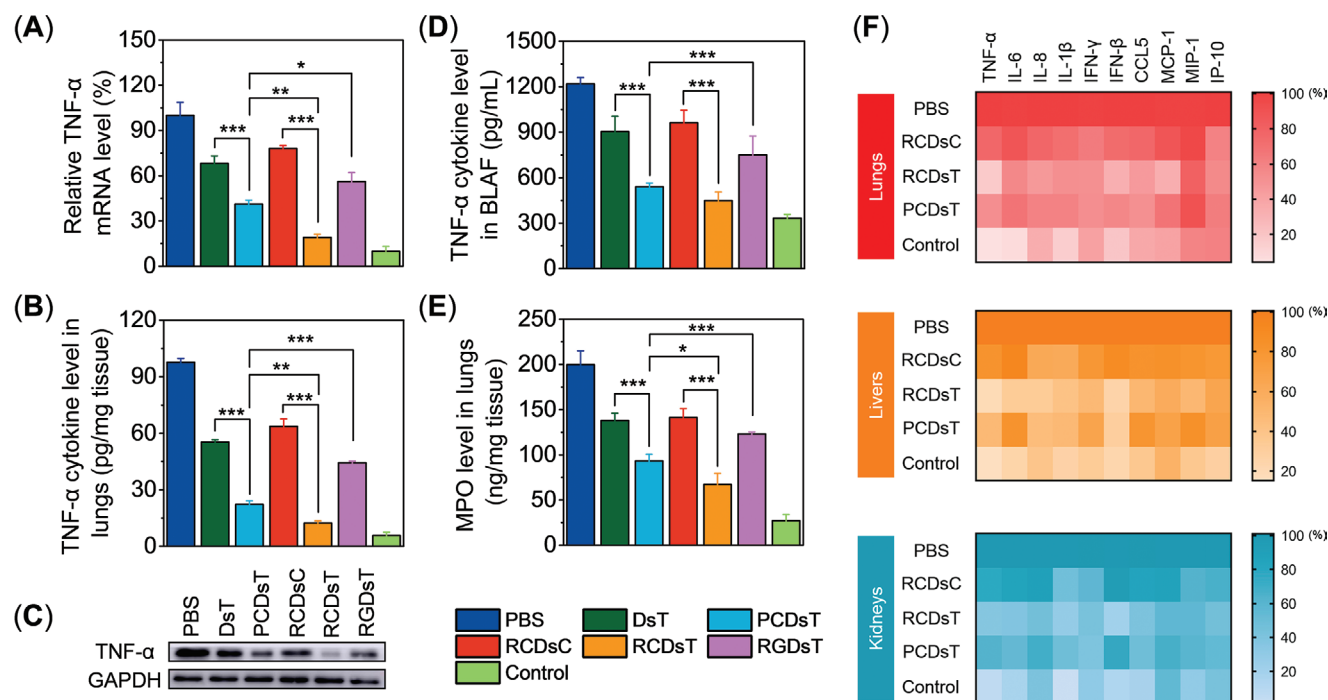
Figure 5. RCDsT NCs mediate potent gene knockdown efficacy against ALI to relieve fulminant cytokine storm. Relative TNF-α mRNA levels (A) and TNF-α protein levels in lung tissues (B) as determined by real-time PCR and ELISA, respectively ($n = 6$). C) Western blot analysis of TNF-α levels in lung tissues. D) TNF-α protein levels in BALF ($n = 6$). E) MPO level in lung tissues ($n = 6$). F) Heatmap of the inflammatory cytokine/chemokine (TNF-α, IL-6, IL-8, IL-1β, IFN-γ, IFN-β, CCL5, MCP-1, MIP-1, and IP-10) levels in lung, liver, and kidney. LPS (1 mg mL^{-1}, 50 μL) is intratracheally injected into mice to induce ALI. 2 h later, PBS or various NCs are intratracheally administered at 150 μg siRNA/kg and 6 mg RC (or RG)/kg. Normal mice without LPS challenge or NCs treatment served as the control. All the above assessments are performed after another 22 h.

reversal capability also provoked higher silencing efficiency (≈60%) than RGDsT NCs (≈45%) that lacked the reversal capability, which further proved that the surface charge reversal of NCs in response to the mild acidity in the inflamed lung tissues could essentially potentiate TNF-α silencing by promoting cellular internalization. Moreover, RCDsT NCs achieved the highest TNF-α mRNA knockdown level (≈80%), significantly outperforming the RCDsC NCs (≈22%, with acid-activated RBP) and PCDsT NCs (≈59%, with siTNF-α), demonstrating the cooperative anti-inflammatory effect of the acid-activated RBP and intracellularly delivered siTNF-α. Similar trend was also noted at the TNF-α protein level in the lung tissues (Figure 5B,C) as well as in bronchoalveolar lavage fluid (BALF, Figure 5D) as determined by ELISA and Western blot analyses. Moreover, the myeloperoxidase (MPO) level in lung tissues was notably decreased following intratracheal administration of NCs, wherein the RCDsT NCs provoked the highest inhibition rate of ≈70% among all tested NCs (Figure 5E). MPO as an inflammation-related enzyme is abundant in neutrophils and macrophages, and MPO inhibition correlates to the amelioration of the inflammatory cascade.[51,52] These results collectively demonstrated that RCDsT NCs were able to realize potent and cooperative anti-inflammatory outcomes following intratracheal administration, as a consequence of their capabilities to efficiently penetrate the mucus layer, undergo charge reversal, and RBP re-activation in the mildly acidic environment of inflamed lung tissues, and finally provoke TNF-α silencing.

During the cytokine storm, pro-inflammatory cytokines such as TNF-α, IL-1β, IL-6, and interleukin-8 (IL-8) serve to activate neutrophils and lymphocytes, increase the permeability of vascular endothelial cells, regulate the metabolic activity of other tissues, and promote the synthesis and release of other cytokines.[2,3] Chemokines, such as chemokine (C−C motif) ligand 5 (CCL5) and monocyte chemotactic protein 1 (MCP-1), display specific chemotactic activities that allow monocytes and macrophages to migrate from blood vessels into the inflamed lesion.[53,54] Interferons, including interferon-γ (IFN-γ) and interferon-β (IFN-β), also play essential roles as biological response modifiers during uncontrolled inflammation.[2] The pro-inflammatory cytokine/chemokine-related feed-forward inflammatory circuit would result in the escalation of cytokine storm.[2,3] Herein, in accordance with the down-regulation of TNF-α, a spectrum of these pro-inflammatory cytokines/chemokines, including IL-1β, IL-6, IL-8, IFN-γ, IFN-β, CCL5, MCP-1, as well as macrophage inflammatory protein 1 (MIP-1), and IFN-γ-induced protein 10 (IP-10), was notably down-regulated following intratracheal administration of NCs, not only in lung but also in liver and kidney. Consistently, RCDsT NCs provoked the highest inhibition rate among all tested NCs (Figure 5F). Such findings, therefore, demonstrated that the RCDsT NCs could efficiently mitigate the pulmonary and systemic cytokine storm during ALI via the cooperative anti-inflammatory effect between siTNF-α and RBP.

**ADVANCED
SCIENCE NEWS**

www.advancedsciencenews.com

**ADVANCED
FUNCTIONAL
MATERIALS**

www.afm-journal.de

Figure 6. RCDsT NCs mediate potent anti-inflammatory efficacy against ALI to recover ventilation functions. Total protein level (A) and total cell count (B) in BALF ($n = 6$). C) The lung wet/dry weight ratios ($n = 6$). pH (D), PaO_2 (E), and $PaCO_2$ (F) in the arterial blood ($n = 6$). G) HE-stained lung sections (scale bar = 200 μm). LPS (1 mg mL^{-1}, 50 μL) is intratracheally injected into mice to induce ALI. 2 h later, PBS or various NCs (PCDsT, RCDsC, and RCDsT, w/w/w = 40/5/1) are intratracheally administered at 150 μg siRNA/kg and 6 mg RC/kg. Normal mice without LPS challenge or NCs treatment served as the control. All the above assessments are performed after another 22 h.

2.6. Recovery of Pulmonary Functions

The capabilities of NCs to attenuate pulmonary pathology and recover ventilation functions were finally evaluated. Increased permeability of the alveolar-capillary barrier is an indicator of ALI, leading to elevated total cell count and protein concentration in the BALF.[26] Pulmonary edema is another important feature of ALI, which could be represented by the enhanced wet/dry weight ratio.[55] Impaired ventilation is the fatal outcome of ALI, as exemplified by the decreased oxygen pressure (PaO_2), increased carbon dioxide pressure ($PaCO_2$), and acidification in the arterial blood.[1] These pathological symptoms were clearly noted in LPS-challenged mice (**Figure 6**A–F), indicating inflammation-induced loss of pulmonary functions and impairment of arterial oxygenation. However, after intratracheal administration of RCDsT NCs, the total cell count and protein level in the BALF, the wet/dry weight ratio of lung tissues, and pH, PaO_2, and $PaCO_2$ in the arterial blood almost completely recovered to the normal levels of mice without LPS challenge, substantiating the potency of RCDsT NCs in restoring pulmonary functions. These findings were further supported by the histological analysis of lung tissues using hematoxylin/eosin (HE) staining, wherein the LPS-induced interstitial edema, destruction of alveolar structure, and thickening of the alveolar wall showed remarkable remission after intratracheal administration of RCDsT NCs (Figure 6G). Moreover, when normal mice were intratracheally injected with

RCDsT NCs, no histological abnormality was noted in HE-stained major organ sections (Figure S18, Supporting Information), indicating unappreciable systemic toxicity of the NCs.

3. Conclusion

In conclusion, we herein presented the first example of trans-mucus siRNA delivery system based on inflammation-instructed charge reversal and surface shedding. RC, an anionic and acid-sheddable pro-peptide of RBP, was designed to coat the DsT NCs and neutralize the positive surface charges, therefore allowing the NCs to efficiently penetrate the mucus layer upon intratracheal administration. In the alveolar spaces with mild acidity, RC transformed back to the native RBP and then shed off to re-expose the positively charged DsT NCs, thereby enabling efficient TNF-α silencing in inflamed lung tissues. As such, siTNF-α and RBP cooperated to alleviate the cytokine storm during ALI. This study, therefore, provides an effective approach for pulmonary siRNA delivery by harmonizing the mucus and cell membrane barriers that used to pose conflicting requirements for materials design. With the potent anti-inflammatory efficacy demonstrated herein, the current study also affords a new tool in the fight against uncontrolled inflammation during severe pneumonia. Considering that various functional PAMAM-based gene delivery systems have been developed to reinforce the transfection efficiencies

in mammalian cells,[56–58] future studies on the structural optimization of DPLL are highly desired to strengthen the gene silencing efficiency of the RCDsT NCs.

4. Experiment Section

Materials, Cells, and Animals: All chemicals were purchased from Aladdin (Shanghai, China) or Energy Chemical (Shanghai, China) unless otherwise specified. RBP was synthesized by Top-Peptide Biotechnology (Nanjing, China), and its amino acid sequence was KLKEKYEKDIAAYRAKGKPDAAKKGVVKAEKSKKKKEC. The G3-PAMAM with 32 terminal primary amines was purchased from Chenyuan Molecular New Material Co. LTD (Weihai, China). zLL-NCA was synthesized according to reported procedures.[47] siTNF-α, siNC with scrambled sequence, and primers were purchased from GenePharma (Shanghai, China), and their sequences were shown in Tables S2 and S3, Supporting Information. LPS (from Escherichia coli 0111:B4) was purchased from Sigma-Aldrich (St. Louis, MO, US). DAPI and Hoechst 33 258 were purchased from Beyotime (Shanghai, China). Lysotracker Red was purchased from Invitrogen (Shanghai, China). Porcine mucin was purchased from Meilun Biotech (Dalian, China). Primary antibodies were purchased from Abcam (Shanghai, China), and secondary antibodies were purchased from Beyotime (Shanghai, China). ELISA kits (TNF-α, IL-6, IL-8, IL-1β, IFN-γ, IFN-β, CCL5, MCP-1, MIP-1, and IP-10) were purchased from Enzyme-linked Biotechnology Co., Ltd. (Shanghai, China). MPO detection kit was purchased from eBioscience (San Diego, CA, USA). RAW 264.7 (mouse monocyte macrophage), MH-S (mouse alveolar macrophages), and Calu-3 (human lung adenocarcinoma) cells were purchased from the American Type Culture Collection and cultured in DMEM supplemented with 10% fetal bovine serum (FBS). Male Balb/c mice (6–8 weeks) were obtained from Shanghai Slaccas Experimental Animal Co., Ltd. and were housed in a clean room, six to a cage. Animal experiments were conducted following protocols approved by Soochow University Laboratory Animal Center, China. The approval number for the laboratory is SYXK(Su)2017-0043.

Synthesis of DPLL: In the glovebox, zLL-NCA (720 mg, 2.37 mmol) was dissolved in *N,N*-dimethylformamide (DMF, 5 mL), and a solution of G3-PAMAM in DMF (20 mg mL^{-1}, 250 µL, 0.024 mmol) was added. The mixture was stirred at room temperature for 3 d. The solution was precipitated from diethyl ether (60 mL), and the white solid was collected by centrifugation and dried under vacuum. The white powder (600 mg) was dissolved in a mixture of trifluoroacetic acid (TFA, 200 mL) and hydrobromic acid/acetic acid (v/v = 2/1, 4 mL). The reaction mixture was stirred at room temperature for 4 h, followed by precipitation using diethyl ether (60 mL). The product was dialyzed against distilled water (MWCO = 1000 Da) for 3 d and lyophilized to obtain DPLL as white solid (565 mg, yield 78%).

Synthesis and Characterization of RG and RC: RBP solution (10 mg mL^{-1}, 2 mL, 7.5 µmol lysine residue) was adjusted to pH 8.5 using NaOH solution (1 M). The solution of CA (23.4 mg mL^{-1} in water, pH 8.5, 1 mL, 2 equiv. of lysine residues in RBP) was slowly added, and the pH was maintained at 8.5. The mixture was stirred at room temperature for 12 h. The resulting mixture was dialyzed (MWCO = 1000 Da) against NaOH solution (pH 8–9) for 12 h and then lyophilized to obtain RC as yellow powder. RG was prepared using the same procedure as RC, where the CA solution was replaced by the glutaric anhydride solution.

The molecular weights (MWs) of RC and RG were determined by MALDI-TOF, and their zeta potentials at pH 7.4 or 6.8 were monitored by Zetasizer Nano ZS90 (Malvern, UK). The graft ratio (%) of CA (or GA) was calculated from the N_{ave}/N_{tot}, where N_{ave} is the average number of CA (or GA) conjugated onto RBP and N_{tot} is the total number of lysine residues in RBP. The bioactivity of RC and RG was determined as follows. RAW 264.7 cells were seeded on 96-well plates (1 × 10^4 cells per well) and incubated for 24 h before cell confluence reached ≈70%. Cells were then incubated with RC, RG, or RBP at different final concentrations (50, 100,

200, 300, and 400 ng µL^{-1}) in opti-MEM (pH 6.8) in the presence of LPS (0.75 ng µL^{-1}, 1 µL) for 24 h. The TNF-α level in the medium was determined by ELISA, and results were denoted as the percentage TNF-α level of control cells that did not receive peptide treatment.

Synthesis and Characterization of poly-$_L$-Lysine (PLL) and PLL-cis-Aconitic Amide (PC): PLL was synthesized using the same procedure as DPLL, wherein the G3-PAMAM solution in DMF was replaced by a solution of hexamethyldisilazane in DMF. Aqueous solution of PLL (10 mg mL^{-1}, 2 mL, 0.14 mmol) was adjusted to pH 8.5 using the NaOH solution (1 M). *cis*-Aconitic anhydride (22 mg/mL in water, pH 8.5, 2 mL, 0.28 mmol) was slowly added, and the pH was maintained at 8.5. The mixture was stirred at room temperature for 12 h. The resulting mixture was dialyzed (MWCO = 1000 Da) against NaOH aqueous solution (pH 8–9) for 12 h and then lyophilized to obtain PC as yellow powder. Its zeta potentials at pH 7.4 or 6.8 were determined by Zetasizer Nano ZS90.

Preparation and Characterization of DsT NCs and RCDsT NCs: For the preparation of binary NCs, DPLL and siTNF-α were separately dissolved in DEPC water (pH 7.4) at 0.5 and 0.1 mg mL^{-1}. DPLL solution was then added to siTNF-α solution at different weight ratios (DPLL/siTNF-α = 0.5/1, 1/1, 2/1, 5/1, 10/1, 15/1, and 20/1). The mixtures were vortexed for 5 s and incubated at 37 °C for 30 min to allow NCs formation. For the preparation of ternary NCs, RC was dissolved in DEPC water (pH 7.4) at 10 mg mL^{-1} and added to freshly prepared DsT NCs (DPLL/siTNF-α = 5/1, w/w) at different weight ratios (RC/siTNF-α = 1/1, 2/1, 5/1, 10/1, 20/1, 30/1, and 40/1). The mixtures were vortexed for 5 s and incubated at 37 °C for 30 min. To evaluate siTNF-α condensation in NCs, freshly prepared NCs were subjected to electrophoresis on 2% agarose gel at 90 V for 20 min. The diameters and zeta potentials of NCs were detected by Zetasizer Nano ZS90. The morphology of DsT NCs (w/w = 5/1) and RCDsT NCs (w/w/w = 40/5/1) were observed by transmission electron microscopy (TEM, TECNAI G2, FEI, US). NCs comprised of the negative control siNC or the non-responsive RG were similarly prepared, and the abbreviations for all tested NCs were listed in Table S1, Supporting Information.

Evaluation of the Stability of RCDsT NCs in CF Sputum: CF sputum was obtained from CF patients of the Second Affiliated Hospital of Soochow University, and was diluted with PBS for 20 folds before use. RCDsT NCs (w/w/w = 40/5/1) were prepared as described above. NCs (10 µL) were mixed with CF sputum (10 µL) and incubated at 37 °C for different time before being subjected to electrophoresis in 2% agarose gel at 90 V for 20 min.

Evaluation of the pH-Sensitivity of RCDsT NCs: RCDsT NCs (w/w/w = 40/5/1) were prepared as described above. Zeta potentials of NCs were determined at different time points following incubation at pH 6.8 or 7.4. The non-responsive RGDsT NCs were used as the control. The FRET assay was also employed to detect the formation and acid-induced dissociation of RCDsT NCs comprised of Cy3-siRNA and Cy5-RC. The freshly prepared RCDsT NCs (w/w/w = 40/5/1) were incubated at pH 6.8 or 7.4 for 30 min, and then the fluorescence spectrum was recorded between 550 and 750 nm with an excitation wavelength of 543 nm. The fluorescence recovery of the donor (Cy3) was used to monitor the dissociation of NCs. The non-responsive RGDsT NCs were used as the control.

Cell Uptake: RAW 264.7 cells were seeded on 96-well plates (1 × 10^4 cells per well) and incubated for 24 h before cell confluence reached ≈70%. Cells were then incubated with RGDsT NCs or RCDsT NCs (w/w/w = 40/5/1) containing FAM-siRNA at 2 µg FAM-siRNA/mL in opti-MEM (pH 6.8 or 7.4) for 4 h. Cells were then washed with cold PBS containing heparin (20 U mL^{-1}) three times and lysed with the RIPA lysis buffer (100 µL well^{-1}). FAM-siRNA content in the lysate was monitored by spectrofluorimetry ($\lambda_{ex}/\lambda_{em}$ = 492/518 nm) and protein level was quantified using the BCA kit. Uptake level was expressed as µg FAM-siRNA associated with 1 mg of cellular protein. The cell uptake of NCs was also evaluated by flow cytometric analysis using similar method.

Intracellular Kinetics: RAW 264.7 cells were seeded on 24-well plates (3 × 10^4 cells per well) and incubated for 24 h before cell confluence reached ≈50%. Cells were then incubated with RGDsT NCs or RCDsT NCs (w/w/w = 40/5/1) comprised of FAM-siRNA and Cy5-RC (or Cy5-RG)

ADVANCED
SCIENCE NEWS

www.advancedsciencenews.com

ADVANCED
FUNCTIONAL
MATERIALS

www.afm-journal.de

at 5 µg FAM-siRNA/mL in opti-MEM (pH 6.8 or 7.4) for 4 h. Cells were then washed with cold PBS containing heparin (20 U mL^{-1}) three times and observed by CLSM. In another study, RAW 264.7 cells on 24-well plates were incubated with RCDsT NCs (w/w/w = 40/5/1) containing FAM-siRNA at 5 µg FAM-siRNA/mL in opti-MEM (pH 6.8) for 2 and 4 h. Cells were then washed with cold PBS containing heparin (20 U mL^{-1}) three times, stained with Hoechst 33 258 (5 µg mL^{-1}) for 30 min and Lysotracker Red (200 nM) for 1 h, and observed by CLSM.

In Vitro TNF-α Knockdown Efficiency in Macrophages: RAW 264.7 cells were seeded on 96-well plates (1 × 10^4 cells per well) and incubated for 24 h before cell confluence reached ≈70%. Cells were then treated with different NCs, including RGDsC, RCDsC, DsT, or RCDsT (w/w = 5/1 for binary NCs and w/w/w = 40/5/1 for ternary NCs), in opti-MEM (pH 6.8) for 4 h at 1 µg siRNA/mL. The medium was then replaced by fresh medium containing 10% FBS, and cells were further cultured for another 20 h before challenge with LPS (7.5 ng mL^{-1}) for 5 h. The TNF-α level in the medium was determined by ELISA, and the knockdown efficiency was denoted as the percentage TNF-α level of control cells that did not receive NCs treatment. To further explore the pH-dependent gene silencing efficiency, RAW 264.7 cells on 96-well plates were treated with various NCs (RGDsC, RCDsC, PCDsT, RGDsT, and RCDsT) at 1 µg siRNA/mL in opti-MEM (pH 6.8 or 7.4) for 4 h. The medium was then replaced by fresh medium containing 10% FBS, and cells were further cultured for another 20 h before challenge with LPS (7.5 ng mL^{-1}) for 5 h. The TNF-α level was determined by ELISA as described above. In addition, the TNF-α mRNA levels in RAW 264.7 or MH-S cells following NCs treatment as described above were determined by real-time PCR at 5 h post LPS challenge.

Cytotoxicity: RAW 264.7 cells were seeded on 96-well plates (1 × 10^4 cells per well) and incubated for 24 h before cell confluence reached ≈70%. Cells were then treated with DsT NCs and RCDsT NCs (RC/siTNF-α = 40/1, w/w) with various DPLL concentrations at 1 µg siTNF-α/mL in opti-MEM for 4 h. The medium was replaced by DMEM containing 10% FBS, and cells were further incubated for 20 h before assessment of cell viability by the MTT assay. Results were presented as percentage viability of control cells that did not receive treatment with NCs. The cytotoxicities of DsT NCs and RCDsT NCs in MH-S cells were determined by the MTT assay using the same method.

MPT in CF Mucus: [35]CF sputum from patients was diluted with PBS for 20 folds. Cy3-siRNA-containing DsT NCs (w/w = 5/1) and RCDsT NCs (w/w/w = 40/5/1) with 2 µg Cy3-siRNA were prepared as described above. NCs (20 µL) were mixed with CF sputum (300 µL) and transferred to custom-made microwells (400 µL) after 30-min equilibrium at 37 °C. 20-s movies at 66.7 ms temporal resolution were acquired by an Evolve 512 EMCCD camera (Photometrics, Tucson, AZ) equipped on an inverted epifluorescence microscope (Observer Z1, Zeiss; Thornwood, NY) with a 100 × 1.4 NA objective. Imaris software was used for the analysis of Brownian movement, and the track of individual NCs was expressed in the form of mean square displacements <MSD> as a function of time scale (τ). Moreover, the distributions of effective diffusivities (D_{eff}) were also counted.

Photobleaching Study: [49]Cy3-siRNA-containing DsT NCs (w/w = 5/1) and RCDsT NCs (w/w/w = 40/5/1) with 2 µg Cy3-siRNA were mixed with mucin solution (0.3% in saline, w/v, 2 mL) as described above. The mixtures were transferred to custom-made microwells (400 µL) after 30-min equilibrium at 37 °C, and observed by an Evolve 512 EMCCD camera (Photometrics, Tucson, AZ) equipped on an inverted epifluorescence microscope (Observer Z1, Zeiss; Thornwood, NY) with a 100 × 1.4 NA objective. Photobleaching was performed in a circular region using the laser beam at 100% laser power and the intensity in the circular region was detected at different time points.

Mucin Aggregation Study: [59]For the measurement of NCs-mucin interaction, Cy3-siRNA-containing DsT NCs (w/w = 5/1) and RCDsT NCs (w/w/w = 40/5/1) with 2 µg Cy3-siRNA were prepared as described above. NCs (20 µL) were mixed with mucin solution (0.1%, 0.3%, or 0.5% in saline, w/v, 2 mL), vortexed, and incubated at 37 °C for 30 min in a shaker. The mixture was centrifuged at 1500 rpm for 2 min and the precipitates were washed twice with PBS. Then, the precipitates were

treated with NaOH (5 M, 200 µL) for 10 min, and the fluorescence intensity was measured ($\lambda_{ex}/\lambda_{em}$ = 550/565 nm).

In Vitro Permeation Across Calu-3 Cell Monolayers: AIC of Calu-3 cells, a well-established in vitro model of bronchial epithelia with secreted mucus layer,[49] was adopted to evaluate the trans-mucus/trans-epithelia penetration of NCs. Briefly, Calu-3 cells were seeded on Transwells (0.33 cm^2, pore size of 3.0 µm, Corning, NY) at 5 × 10^5 cell cm^{-2} and cultured for 14 d. The TEER value was daily measured during days 7 to 14. The medium in the apical compartment was removed on day 4 while the medium in the basolateral side was refreshed every day. When the TEER value reached 700 Ω·cm^2 (usually within 14 d), the cell monolayers were used for the permeation studies. Hank's balanced salt solution (HBSS, 500 µL) containing 1% BSA was added to the basolateral side, and Cy3-siRNA-containing DsT NCs (w/w = 5/1) and RCDsT NCs (w/w/w = 40/5/1) with 6 µg Cy3-siRNA were added to the apical side in HBSS (200 µL) containing 1% BSA. After incubation at 37 °C for 6 h, the medium in the basolateral side was harvested, and the amount of Cy3-siRNA was determined by spectrofluorimetry ($\lambda_{ex}/\lambda_{em}$ = 550/565 nm). The penetrating capabilities of the NCs were represented by the P_{app} using the equation of $P_{app} = Q/Act$, where Q is the amount of permeated Cy3-siRNA (ng), A is the diffusion area of the cell monolayers (cm^2), c is the initial concentration of Cy3-siRNA at the apical side (ng cm^{-3}), and t is the transport time (s).

To determine the transfection capabilities of RCDsT NCs following transport across Calu-3 cell monolayers, RCDsT NCs were incubated with cell monolayers for 4 h as described above. The medium in the basolateral side was harvested and was used to treat RAW 264.7 cells as described above at pH 6.8 and 1 µg siRNA/mL followed by LPS challenge. The TNF-α mRNA levels in RAW 264.7 cells were determined by real-time PCR, and freshly prepared RCDsT NCs before the transport study were used as the control.

In Vivo Mucus Penetration and Pulmonary Distribution: Male Balb/c mice were intratracheally injected with LPS solution (1 mg/mL in saline, 50 µL) to induce ALI. At 2 h post LPS challenge, DsT NCs (w/w = 5/1, 20 µL) and RCDsT NCs (w/w/w = 40/5/1, 20 µL) containing Cy3-siRNA were intratracheally injected at 150 µg Cy3-siRNA/kg. 1 h later, animals were sacrificed and lung tissues were collected, washed with PBS, embedded in OCT, cryo-sectioned at 10-µm thickness, stained with DAPI for 10 min, and observed by CLSM.

Biodistribution Analysis: Male Balb/c mice were randomly divided into three groups (six mice per group), and were intratracheally injected with LPS solution (1 mg mL^{-1} in saline, 50 µL) to induce ALI. At 2 h post LPS challenge, DsT NCs (w/w = 5/1, 20 µL) and RCDsT NCs (w/w/w = 40/5/1, 20 µL) containing Cy5-siRNA were intratracheally administered at 150 µg siRNA/kg and 6 mg RC (or RG)/kg. Mice were euthanized and the major organs (liver, spleen, lung, heart, kidney) were harvested at 4 and 24 h post intratracheal administration. Isolated tissues were subjected to ex vivo fluorescence imaging using the Maestro in vivo optical imaging system (Cambridge Research and Instrumentation, Inc.).

In Vivo Gene Knockdown Efficiency: Male Balb/c mice were randomly divided into seven groups (six mice per group). LPS was intratracheally injected to induce ALI. At 2 h post LPS challenge, PBS or various NCs (DsT, PCDsT, RCDsC, RCDsT, and RGDsT, w/w = 5/1 for binary NCs and w/w/w = 40/5/1 for ternary NCs, 20 µL) were intratracheally administered at 150 µg siRNA/kg and 6 mg RC (or RG)/kg. Normal mice without LPS challenge and NCs treatment served as the control. Animals were sacrificed at 22 h post-administration of NCs, and lung tissues were harvested and washed with PBS. The obtained lung tissues were homogenized using the Trizol reagent to collect total RNA, and the TNF-α mRNA level was determined by real-time PCR. The lung tissues were also homogenized using the passive lysis buffer containing protease inhibitor. The homogenate was centrifuged at 15 000 rpm and 4 °C for 10 min, and the supernatant was subjected to the determination of TNF-α level using ELISA kits. The TNF-α level in lung tissues was also monitored by Western blot analysis. In particular, the collected lung tissues were homogenized in passive lysis buffer and centrifuged at 15 000 rpm and 4 °C for 10 min. The Western blot assay was carried out by fractionating the supernatant on SDS-PAGE, blotting to nitrocellulose

membranes, blocking with 5% non-fat dry milk in $1 \times$ TBS containing 1% Tween 20 for 1 h, incubating with primary antibodies overnight at 4 °C, incubating with secondary antibody, and analyzing by an enhanced chemiluminescence detection system. The concentrations of each antibody used were 1:1000 (anti-TNF-α), 1:1000 (anti-GAPDH), and 1:500 (secondary antibody).

Anti-Inflammatory Efficacy against Cytokine Storm In Vivo: Male Balb/c mice were randomly divided into five groups (six mice per group). LPS was intratracheally injected to induce ALI. At 2 h post LPS challenge, PBS or various NCs (PCDsT, RCDsC, and RCDsT, w/w/w = 40/5/1, 20 μL) were intratracheally administered at 150 μg siRNA/kg and 6 mg RC/kg. Normal mice without LPS challenge and NCs treatment served as the control. Animals were sacrificed at 22 h post-administration of NCs, and lung, liver, and kidney were harvested and washed with PBS. The tissues were homogenized using passive lysis buffer containing protease inhibitor. The homogenate was centrifuged at 15 000 rpm and 4 °C for 10 min, and the supernatant was subjected to quantification of inflammatory cytokine/chemokine levels using ELISA kits, including IL-8, IL-6, IL-1β, IFN-γ, IFN-β, CCL5, MCP-1, MIP-1, and IP-10.

BALF Collection and Analysis: [26]The BALF was collected at 22 h post-NCs administration, and it was centrifuged at 15 000 rpm and 4 °C for 10 min. The supernatant was collected and subjected to the measurement of TNF-α level using the ELISA kit and total protein level using the BCA kit. The cell pellets were re-suspended in PBS to allow for total cell counting.

MPO Levels in Lung Tissues: [26]MPO level in the lung tissues was also measured to indicate neutrophil recruitment. Briefly, lung tissues were collected at 22 h post-NCs administration and homogenized with the passive lysis buffer. The homogenate was centrifuged at 15 000 rpm and 4 °C for 10 min before quantification of the MPO activity in the supernatant using the MPO mouse ELISA kit.

Measurement of Wet/Dry Weight Ratio of Lung Tissues: [55]The water content in the lung tissues was determined by calculating the wet/dry weight ratio. The lung tissues were collected at 22 h post-NCs administration, washed with PBS, and weighed to obtain the "wet" weight. The lung tissues were then dried at 80 °C for 72 h to obtain the "dry" weight, and the wet/dry weight ratio was accordingly calculated.

Blood Gas Analysis: Blood samples were obtained from the arterial carotids at 22 h post-NCs administration, and were directly subjected to the measurement of PaO$_2$, PaCO$_2$, and pH by using the blood-gas analyzer (Radiometer, Shanghai, China).

Histological Assessment: The lung tissues were harvested at 22 h post intratracheal administration of NCs, fixed in 10% neutral buffered formalin, embedded in paraffin, sectioned at 8-μm thickness, and stained with HE before histological observation using optical microscopy.

Biocompatibility Assessment: RCDsT NCs (40/5/1, 20 μL) were intratracheally injected into normal male Balb/c mice at 150 μg siRNA/kg and 6 mg RC/kg. PBS was injected as the control. Mice were euthanized 24 h later, and major organs including liver, spleen, kidney, lung, heart, and brain were harvested, fixed in 10% neutral buffered formalin, embedded in paraffin, sectioned at 8-μm thickness, and stained with HE before histological observation using optical microscopy.

Statistical Analysis: Data were expressed as mean ± standard deviation unless otherwise indicated. Statistical comparisons were made in the Prism software using a Student's *t*-test (for two groups meeting the normal distribution criteria) or ANOVA with Tukey's multiple comparison test (for groups across variables, with multiple comparisons between groups). For Student's *t*-test, differences were assessed to be significant at $*p < 0.05$ and very significant at $**p < 0.01$ and $***p < 0.001$. For ANOVA test, differences were assessed to be significant at $\#p < 0.05$ and very significant at $\#\#p < 0.01$.

Supporting Information

Supporting Information is available from the Wiley Online Library or from the author.

Conflict of Interest

The authors declare no conflict of interest.

Data Availability Statement

Research data are not shared.

[1] M. A. Matthay, R. L. Zemans, G. A. Zimmerman, Y. M. Arabi, J. R. Beitler, A. Mercat, M. Herridge, A. G. Randolph, C. S. Calfee, *Nat. Rev. Dis. Primers* **2019**, *5*, 18.

[2] P. Mehta, D. F. McAuley, M. Brown, E. Sanchez, R. S. Tattersall, J. J. Manson, H. L. H. A. Speciality, *Lancet* **2020**, *395*, 1033.

[3] Q. Liu, Y. H. Zhou, Z. Q. Yang, *Cell. Mol. Immunol.* **2016**, *13*, 3.

[4] C. C. Mello, D. Conte, *Nature* **2004**, *431*, 338.

[5] C. Yin, S. Ackermann, Z. Ma, S. Mohanta, C. Zhang, Y. Li, S. Nietzsche, M. Westermann, L. Peng, D. Hu, S. Bontha, P. Srikakulapu, M. Beer, R. Megens, S. Steffens, M. Hildner, L. Halder, H. Eckstein, J. Pelisek, J. Herms, S. Roeber, T. Arzberger, A. Borodovsky, L. Habenicht, C. Binder, C. Weber, P. Zipfel, C. Skerka, A. Habenicht, *Nat. Med.* **2019**, *25*, 496.

[6] M. P. Lokugamage, Z. Gan, C. Zurla, J. Levin, F. Z. Islam, S. Kalathoor, M. Sato, C. D. Sago, P. J. Santangelo, J. E. Dahlman, *Adv. Mater.* **2020**, *32*, 1904905.

[7] L. Rackley, J. Stewart, J. Salotti, A. Krokhotin, A. Shah, J. Halman, R. Juneja, J. Smollett, L. Lee, K. Roark, M. Viard, M. Tarannum, J. Vivero-Escoto, P. Johnson, M. Dobrovolskaia, N. Dokholyan, E. Franco, K. A. Afonin, *Adv. Funct. Mater.* **2018**, *28*, 1805959.

[8] K. Whitehead, J. Dorkin, A. Vegas, P. Chang, O. Veiseh, J. Matthews, O. Fenton, Y. Zhang, K. Olejnik, V. Yesilyurt, D. Chen, S. Barros, B. Klebanov, T. Novobrantseva, R. Langer, D. Anderson, *Nat. Commun.* **2014**, *5*, 4277.

[9] J. Zhuang, H. Gong, J. Zhou, Q. Zhang, W. Gao, R. Fang, L. Zhang, *Sci. Adv.* **2020**, *6*, eaaz6108.

[10] D. Wang, J. Lin, F. Jia, X. Tan, Y. Wang, X. Sun, X. Cao, F. Che, H. Lu, X. Gao, J. C. Shimkonis, Z. Nyoni, X. Lu, K. Zhang, *Sci. Adv.* **2019**, *5*, eaav9322.

[11] S. Liang, X. Z. Yang, X. J. Du, H. X. Wang, H. J. Li, W. W. Liu, Y. D. Yao, Y. H. Zhu, Y. C. Ma, J. Wang, E. W. Song, *Adv. Funct. Mater.* **2015**, *25*, 4778.

[12] K. M. McMahon, M. P. Plebanek, C. S. Thaxton, *Adv. Funct. Mater.* **2016**, *26*, 7824.

**ADVANCED
SCIENCE NEWS**
www.advancedsciencenews.com

**ADVANCED
FUNCTIONAL
MATERIALS**
www.afm-journal.de

[13] Y. Guo, Z. Wu, S. Shen, R. Guo, J. Wang, W. Wang, K. Zhao, M. Kuang, X. Shuai, *Nat. Commun.* **2018**, *9*, 3430.

[14] O. F. Khan, P. S. Kowalski, J. C. Doloff, J. K. Tsosie, V. Bakthavatchalu, C. B. Winn, J. Haupt, M. Jamiel, R. Langer, D. G. Anderson, *Sci. Adv.* **2018**, *4*, eaar8409.

[15] R. Kedmi, N. Veiga, S. Ramishetti, M. Goldsmith, D. Rosenblum, N. Dammes, I. Hazan-Halevy, L. Nahary, S. Leviatan-Ben-Arye, M. Harlev, M. Behlke, I. Benhar, J. Lieberman, D. Peer, *Nat. Nanotechnol.* **2018**, *13*, 214.

[16] Y. Z. Dong, K. T. Love, J. R. Dorkin, S. Sirirungruang, Y. L. Zhang, D. L. Chen, R. L. Bogorad, H. Yin, Y. Chen, A. J. Vegas, C. A. Alabi, G. Sahay, K. T. Olejnik, W. H. Wang, A. Schroeder, A. K. R. Lytton-Jean, D. J. Siegwart, A. Akinc, C. Barnes, S. A. Barros, M. Carioto, K. Fitzgerald, J. Hettinger, V. Kumar, T. I. Novobrantseva, J. N. Qin, W. Querbes, V. Koteliansky, R. Langer, D. G. Anderson, *Proc. Natl. Acad. Sci. USA* **2014**, *111*, 3955.

[17] Y. F. Yan, L. Liu, H. Xiong, J. B. Miller, K. J. Zhou, P. Kos, K. E. Huffman, S. Elkassih, J. W. Norman, R. Carstens, J. Kim, J. D. Minna, D. J. Siegwart, *Proc. Natl. Acad. Sci. USA* **2016**, *113*, E5702.

[18] J. Conde, C. Bao, Y. Tan, D. Cui, E. Edelman, H. Azevedo, H. Byrne, N. Artzi, F. Tian, *Adv. Funct. Mater.* **2015**, *25*, 4183.

[19] S. Ramishetti, I. Hazan-Halevy, R. Palakuri, S. Chatterjee, S. Naidu Gonna, N. Dammes, I. Freilich, L. Kolik Shmuel, D. Danino, D. Peer, *Adv. Mater.* **2020**, *32*, 1906128.

[20] J. J. Nie, B. K. Qiao, S. Duan, C. Xu, B. Y. Chen, W. J. Hao, B. R. Yu, Y. L. Li, J. Du, F. J. Xu, *Adv. Mater.* **2018**, *30*, 1801570.

[21] C. Xu, Y. Zhang, K. Xu, J. Nie, B. Yu, S. Li, G. Cheng, Y. Li, J. Du, F. J. Xu, *Nat. Commun.* **2019**, *10*, 3184.

[22] H. S. Kim, Y. J. Son, W. Mao, K. W. Leong, H. S. Yoo, *Nano Lett.* **2018**, *18*, 314.

[23] H. X. Wang, Z. Y. Song, Y. H. Lao, X. Xu, J. Gong, D. Cheng, S. Chakraborty, J. S. Park, M. Q. Li, D. T. Huang, L. C. Yin, J. J. Cheng, K. W. Leong, *Proc. Natl. Acad. Sci. USA* **2018**, *115*, 4903.

[24] R. Q. Li, Y. N. Wu, Y. Zhi, X. C. Yang, Y. L. Li, F. J. Xu, J. Du, *Adv. Mater.* **2016**, *28*, 7204.

[25] Y. Ju, C. Cortez-Jugo, J. Chen, T. Wang, A. Mitchell, E. Tsantikos, N. Bertleff-Zieschang, Y. Lin, J. Song, Y. Cheng, S. Mettu, M. Rahim, S. Pan, G. Yun, M. Hibbs, L. Yeo, C. Hagemeyer, F. Caruso, *Adv. Sci.* **2020**, *7*, 1902650.

[26] C. Ge, J. Yang, S. Duan, Y. Liu, F. Meng, L. Yin, *Nano Lett.* **2020**, *20*, 1738.

[27] A. K. Patel, J. C. Kaczmarek, S. Bose, K. J. Kauffman, F. Mir, M. W. Heartlein, F. DeRosa, R. Langer, D. G. Anderson, *Adv. Mater.* **2019**, *31*, 1805116.

[28] D. P. Feldmann, Y. L. Cheng, R. Kandil, Y. R. Xie, M. Mohammadi, H. Harz, A. Sharma, D. J. Peeler, A. Moszczynska, H. Leonhardt, S. H. Pun, O. M. Merkel, *J. Controlled Release* **2018**, *276*, 50.

[29] A. da Silva, G. de Oliveira, N. Kim, F. Cruz, J. Kitoko, N. Blanco, S. Martini, J. Hanes, P. Rocco, J. Suk, M. Morales, *Sci. Adv.* **2020**, *6*, eaay7973.

[30] C. Bao, B. Liu, B. Li, J. Chai, L. Zhang, L. Jiao, D. Li, Z. Yu, F. Ren, X. Shi, Y. Li, *Nano Lett.* **2020**, *20*, 1352.

[31] C. Menzel, A. Bernkop-Schnuerch, *Adv. Drug Delivery Rev.* **2018**, *124*, 164.

[32] I. Nazir, A. Fürst, N. Lupo, A. Hupfauf, R. Gust, A. Bernkop-Schnürch, *Eur. J. Pharm. Biopharm.* **2019**, *144*, 40.

[33] A. Bernkop-Schnuerch, *Adv. Drug Delivery Rev.* **2018**, *136*, 62.

[34] N. S. Chen, M. Zhou, X. Dong, J. M. Qu, F. Y. Gong, Y. Han, Y. Qiu, J. L. Wang, Y. Liu, Y. Wei, J. A. Xia, T. Yu, X. X. Zhang, L. Zhang, *Lancet* **2020**, *395*, 507.

[35] P. Mastorakos, A. L. da Silva, J. Chisholm, E. Song, W. K. Choi, M. P. Boyle, M. M. Morales, J. Hanes, J. S. Suk, *Proc. Natl. Acad. Sci. USA* **2015**, *112*, 8720.

[36] S. Lai, D. O'Hanlon, S. Harrold, S. Man, Y. Wang, R. Cone, J. Hanes, *Proc. Natl. Acad. Sci. USA* **2007**, *104*, 1482.

[37] A. J. Kim, N. J. Boylan, J. S. Suk, M. Hwangbo, T. Yu, B. S. Schuster, L. Cebotaru, W. G. Lesniak, J. S. Oh, P. Adstamongkonkul, A. Y. Choi, R. M. Kannan, J. Hanes, *Angew. Chem., Int. Ed.* **2013**, *52*, 3985.

[38] B. Tang, M. Dawson, S. Lai, Y. Wang, J. Suk, M. Yang, P. Zeitlin, M. Boyle, J. Fu, J. Hanes, *Proc. Natl. Acad. Sci. USA* **2009**, *106*, 19268.

[39] L. Dai, K. Li, M. Li, X. Zhao, Z. Luo, L. Lu, Y. Luo, K. Cai, *Adv. Funct. Mater.* **2018**, *28*, 1707249.

[40] X. D. Xu, P. E. Saw, W. Tao, Y. J. Li, X. Y. Ji, M. Yu, M. Mahmoudi, J. Rasmussen, D. Ayyash, Y. X. Zhou, O. C. Farokhzad, J. J. Shi, *Nano Lett.* **2017**, *17*, 4427.

[41] J. Li, X. Yu, X. Wang, Y. Yuan, H. Xiao, D. Cheng, X. Shuai, *Adv. Mater.* **2014**, *26*, 8217.

[42] S. Mura, J. Nicolas, P. Couvreur, *Nat. Mater.* **2013**, *12*, 991.

[43] J. H. Song, J. Y. Kim, C. Piao, S. Lee, B. Kim, S. J. Song, J. S. Choi, M. Lee, *J. Controlled Release* **2016**, *234*, 33.

[44] S. Lee, C. Piao, G. Kim, J. Kim, E. Choi, M. Lee, *Eur. J. Pharm. Sci.* **2018**, *114*, 275.

[45] E. Choi, J. Oh, D. Lee, J. Lee, X. Tan, M. Kim, G. Kim, C. Piao, M. Lee, *J. Controlled Release* **2018**, *279*, 40.

[46] K. S. Sfanos, S. Yegnasubramanian, W. G. Nelson, A. M. De Marzo, *Nat. Rev. Urol.* **2018**, *15*, 11.

[47] H. Fang, Z. Guo, L. Lin, J. Chen, P. Sun, J. Wu, C. Xu, H. Tian, X. Chen, *J. Am. Chem. Soc.* **2018**, *140*, 11992.

[48] Q. Cheng, T. Wei, Y. Jia, L. Farbiak, K. Zhou, S. Zhang, Y. Wei, H. Zhu, D. J. Siegwart, *Adv. Mater.* **2018**, *30*, 1805308.

[49] X. Zhu, J. Wu, W. Shan, Z. Zhou, M. Liu, Y. Huang, *Adv. Funct. Mater.* **2016**, *26*, 2728.

[50] Y. Liu, Y. Zou, C. Feng, A. Lee, J. Yin, R. Chung, J. Park, H. Rizos, W. Tao, M. Zheng, O. Farokhzad, B. Shi, *Nano Lett.* **2020**, *20*, 1637.

[51] A. Haegens, J. Vernooy, P. Heeringa, B. Mossman, E. Wouters, *Eur. Respir. J.* **2008**, *31*, 252.

[52] N. Zhang, K. Francis, A. Prakash, D. Ansaldi, *Nat. Med.* **2013**, *19*, 500.

[53] M. Merad, J. Martin, *Nat. Rev. Immunol.* **2020**, *20*, 355.

[54] F. Marra, F. Tacke, *Gastroenterology* **2014**, *147*, 577.

[55] B. Patel, M. Wilson, M. Takata, *Eur. Respir. J.* **2012**, *39*, 1162.

[56] J. Wang, R. Cooper, H. Yang, *Biomacromolecules* **2020**, *21*, 4008.

[57] D. Wang, J. Wang, J. Song, Q. Shen, R. Wang, W. Lu, J. Pan, C. Xie, M. Liu, *J. Gene Med* **2020**, *22*, e3240.

[58] D. Wang, J. Song, J. Wang, Z. Zhang, Q. Shen, J. Wang, H. Guo, R. Wang, C. Xie, W. Lu, M. Liu, *Adv. Funct. Mater.* **2020**, *30*, 2004783.

[59] W. Shan, X. Zhu, M. Liu, L. Li, J. Zhong, W. Sun, Z. Zhang, Y. Huang, *ACS Nano* **2015**, *9*, 2345.